

Tuning of Interlayer Coupling in Large-Area Graphene/WSe₂ van der Waals Heterostructure via Ion Irradiation: Optical Evidences and Photonic Applications

Yang Tan[†], Xiaobiao Liu[†], Zhiliang He[‡], Yanran Liu[†], Mingwen Zhao^{†}, Han Zhang^{‡*}, and Feng Chen^{†*},*

[†]School of Physics, State Key Laboratory of Crystal Materials, Shandong University, Shandong, Jinan, 250100, China,

[‡]Shenzhen Key Laboratory of two dimensional materials and devices, Shenzhen Engineering Laboratory of Phosphorene and Optoelectronics, Key Laboratory of Optoelectronic Devices and Systems of Ministry of Education and Guangdong Province, Shenzhen University, Shenzhen 518060, China

KEYWORDS: Heterostructure, graphene/WSe₂, interlayer coupling, ion irradiation, 2D materials, Q-switched lasing.

ABSTRACT:

Van der Waals (vdW) heterostructures are receiving great attentions due to their intriguing properties and potentials in many research fields. The flow of charge carriers in vdW heterostructures can be efficiently rectified by the inter-layer coupling between neighboring layers, offering a rich collection of functionalities and a mechanism for designing atomically thin devices. Nevertheless, non-uniform contact in larger-area heterostructures reduces the device efficiency. In this work, ion irradiation had been verified as an efficient technique to enhance the contact and interlayer coupling in the newly developed graphene/WSe₂ heterostructure with a large area of 10 mm × 10 mm. During the ion irradiation process, the morphology of monolayer graphene had been modified, promoting the contact with WSe₂. Experimental evidences of the tunable interlayer electron transfer are displayed by investigation of photoluminescence and ultrafast absorption of the irradiated heterostructure. Besides, we have found that in graphene/WSe₂ heterostructure, graphene serves as a fast channel for the photo-excited carriers to relax in WSe₂, and the nonlinear absorption of WSe₂ could be effectively tuned by the carrier transfer process in graphene, enabling specific optical absorption of the heterostructure in comparison with separated graphene or WSe₂. On the basis of these new findings, by applying the ion beam modified graphene/WSe₂ heterostructure as a saturable absorber, Q-switched pulsed lasing with optimized performance has been realized in a Nd:YAG waveguide cavity. This work paves the way towards developing novel devices based on large-area heterostructures by using ion beam irradiation.

In parallel with research wave of graphene and other two-dimensional (2D) atomic crystals, heterostructures have attracted an increasingly attention over the past decade¹⁻³. Heterostructures are layered materials bonded by the van der Waals (vdW) force, which are assembled by stacking different 2D materials on the top of each other⁴. The stacked layers with an artificial sequence can be employed to engineer the electronic band structures, allowing the interlayer electronic tunneling. The transition of electrons within an artificially designed energy barrier offers 2D heterostructures with exotic optical functionalities⁵, including enhanced saturable absorption⁶, ultrafast photo-responses⁷, and modulated photoluminescence (PL)⁸. The performance of these unique incremental functions depends on the efficiency of electronic tunneling (i.e., the interlayer coupling) between the distinct 2D materials of the heterostructures⁹⁻¹¹.

However, as the layered materials are combined by the vdW force (considerably weak in comparison to the covalent bond), it is quite difficult to obtain an intense contact. Extra spaces, e.g. the trapped residual molecules and ripples (deformation) on 2D materials formed during the mechanical transfer or fabrication processes¹², also exist in the interlayer space. The loose contact reduces the interlayer coupling of heterostructures which hampers the development of large-area heterostructures. Recently, thermal annealing was used to drive the trapped residual molecules out of the interlayer space and thus improve the layers the interlayer coupling between the MoS₂ and WS₂ monolayers¹³. However, ripples (deformation) on 2D materials could not be flattened by simply annealing. It is urgent to seek efficient methods to minimize ripples for the further development and application of the heterostructure.

As one of the most intriguing applications in photonics, 2D materials have been widely applied in ultrafast laser generation as broadband saturable absorbers^{14,15}. Due to different electronic structures of 2D materials, they have different performances of the saturable absorption. For instance, graphene has an ultrafast recovery time (relaxation time less than 150 fs) allowing a fast response in a laser system, but the optical modulation depth is low (around 1% for the monolayer graphene). Topological

insulators (TI, e.g., Bi₂Se₃, Bi₂Te₃ and Sb₂Te₃) and transition metal dichalcogenides (TMDC, e.g. WSe₂, WS₂, MoS₂) have a high modulation depth, but the relaxation time is quite long (more than 500 fs) demonstrating a slow saturable absorber. One potential solution to complement advantages of TI (or TMDC) and graphene is to constitute heterostructure with graphene and other 2D materials. However, graphene has intrinsic ripples or corrugations because of thermal fluctuations¹⁶, leading to the loose contact between neighbor layers and further hamper the interlayer coupling in the heterostructure. Recently, direct growing the thin nanocrystals on graphene substrate is reported as a method to constitute the heterostructure with a good interlayer coupling. But, this method only applies for limited materials and has stringent requirements for experimental operations. Besides, it cannot control the number of layers in the nanocrystal and the roughness of the heterostructure. Therefore, it is still desirable to explore new techniques to enhance interlayer coupling between graphene and 2D materials^{6,17,18} for the further development of high-quality heterostructures.

The ion beam technology has been proved to be an effective way to modify the properties and functions of 2D materials. For example, ion irradiation could induce defects in 2D materials to realize effective tuning of their electronic structures and optical properties through carefully choosing irradiation conditions (e.g., ion species, energy, and fluence)¹⁹⁻²¹. In this work, we demonstrate the ion irradiation as an efficient tool to enhance the interlayer coupling, which enables efficient tailoring of optical functions of the heterostructures. The new-developed heterostructure used in this work consist of a monolayer graphene and WSe₂ (Tungsten-based dichalcogenide). By changing the fluence of ion beam, the average interlayer distance of the heterostructure is significantly decreased from ~4nm to ~0.2 nm with a minimal damage to structures of graphene and WSe₂. As the interlayer distance decreases, the interlayer coupling of the heterostructure has been enhanced considerably. Based on these findings, graphene/WSe₂ heterostructure is used as the saturable absorber for the Q-switched pulsed laser generation. Our work indicates ion irradiation as a novel way to tailor optical properties of the heterostructures.

The atomic force microscope (AFM) topographic data of the as-prepared graphene/WSe₂ heterostructure is shown in Figure 1a. As graphene is mechanically stacked onto monolayer WSe₂, there are ripples and corrugations on the transferred monolayer graphene due to the intrinsic thermal fluctuations and the transfer process (Figure 1b), resulting in a loose contact between layers (Figure 1c). Taking the thickness of the as-prepared heterostructure (~5 nm), graphene (~0.24 nm) and WSe₂ (~0.7 nm)^{22,23} into account, the average interlayer distance is ~4 nm. After the carbon ion irradiation, the morphology of graphene/WSe₂ heterostructure could be modified (Figure 1d), leading to intense contact with the average thickness of 1.1nm. Considering the thickness of graphene and WSe₂ layers, the interlayer distance is determined to be ~0.2 nm after the ion irradiation, demonstrating the graphene/WSe₂ heterostructure has been compressed during the ion irradiation process (Figure 1e and 1f). More interestingly, the interlayer distance can be tailored by the fluence of the incident carbon ions. The interlayer distance has been gradually changed from 4 nm to 0.2 nm along with the increasing of the ion fluence (Figure 1g).

During the ion irradiation process, incident energetic ions pass through the heterostructure and have been injected into the substrate. Through the interaction with the heterostructure, the incident ions are slow down and transfer energy to the heterostructure. Meanwhile, a large number of near-surface atoms in the heterostructure are excited and obtain the momentum along with the direction of the incident ions. As a result, adjacent layers approach to each other, which decrease the interlayer distance of the heterostructure. In addition, the ripples and corrugations are transformed to tiny wrinkles after the irradiation. The evidence for the ion irradiation induced compression can be found in the Raman spectrum. The G-band of graphene represents the phonon modes between carbon atoms, which is sensitive to the state of stress, strain and the lattice disorder induced by compression. Figure 1h display the comparison of Raman signals of as-prepared and irradiated graphene/WSe₂ heterostructure. Raman peaks of graphene have the red shift after irradiation, demonstrating the graphene monolayer is compressed during the ion irradiation process.²⁴

The quality of the heterostructure before and after the irradiation is also characterized by the Raman spectrum within the band of 100 nm–400 nm (WSe₂) and 1000 nm–3000 nm (graphene) in Figure 1h. For the WSe₂ layer, the position of the Raman peak (P) remains at 252.6 nm, while the bandwidth (W) of Raman signal of the as-prepared and irradiated ones is slight increased from 6.5cm⁻¹ (S_0) to 7.7 cm⁻¹ (S_3), indicatting after the irradiation, the intrinsic structure of WSe₂ were well-preserved. For graphene, the G and $2D$ peaks in the as-prepared sample have the intensity ratio of 0.4 (I_G/I_{2D}), implying the nature of monolayer graphene²⁰. The ratio of D and G peaks demonstrates the density of the zero-dimensional point-like defects in graphene. And the tiny value of D/G ratio also indicates the excellent quality of graphene in the as-prepared one²³. Based on these results, one can conclude that both graphene and WSe₂ monolayer are not damaged during the irradiation.

According to previous discussion, the ion irradiation process can change the morphology of graphene, resulting in a close contact with the WSe₂ layer and consequently enhancement of interlayer coupling. This allows us to investigate the tuning effect of interlayer coupling, according to the measured optical functions of the heterostructures.

Figure 2a shows the normalized PL spectra emerged from the monolayer WSe₂ (orange line), heterostructures before (red line) and after ion irradiation (blue line), respectively. Dominated by the A excitation, the PL spectrum of the WSe₂ monolayer has a remarkable exciton emission at 748 nm, which is consistent with the previous study²⁵. In contrast to the WSe₂, the PL spectrum of as-prepared heterostructure has little change in the shape, indicating an undisturbed energy state of the WSe₂ and a weak interaction between graphene and the monolayer WSe₂. After ion irradiation, the PL spectrum shows a remarkable band broadening and the blue shift (1 nm) of peak position. These notable variations may imply that the irradiation enhances the interlayer coupling and modifies the electronic structure of the graphene/WSe₂ heterostructure. Further evidence for the enhanced interlayer coupling is observed in the time-resolved PL decay kinetics characterization (Figure 2b) at 748 nm.

Before the irradiation, the as-prepared heterostructure has the same decay time as WSe₂ layer (2.45 ns), whilst the irradiated heterostructure possesses a faster decay (2.2 ns), suggesting an acceleration of charge transfer in WSe₂ due to the enhancement of interlayer coupling. Figure 2d and 2e are the PL mappings of the heterostructure before (Figure 2d) and after (Figure 2e) the ion irradiation at 748 nm.

In order to reveal the relationship between the interlayer coupling and the charge transfer in 2D materials, we have detected charge/excitons transfer of the irradiated heterostructure and two components (graphene monolayer and WSe₂ monolayer) through the pump - probe measurement by using a mode-locked Yb:KGW fiber laser (190 fs, 515 nm, 20 Hz)²⁶. As shown in Figure 2f, the single-exponential decay with a time constant of 2.4ps/10ps indicates the ultrafast/slow carrier lifetime in graphene/WSe₂. More interestingly, similar experiment with the irradiated heterostructure (Figure 2f) exhibits two astonishing features. First, the magnitude of the signal (1.3) is 10 times higher than the monolayer WSe₂ and graphene, respectively. Second, the delay time (2.4 ps) is much shorter than the WSe₂ monolayer but close to that of graphene. These observations imply that the irradiated heterostructure possesses advantages of both graphene and WSe₂ monolayer due to the enhanced interlayer coupling. In respect to the isolated graphene/WSe₂, the heterostructure exhibits stronger and faster charge transfer effect.

To provide an insight into the observed phenomena, we performed first-principles calculations within the density-functional theory (DFT) of the graphene/WSe₂ heterostructure using the Vienna ab initio simulation package known as the VASP code²⁷⁻²⁹. The heterostructure is modeled by placing a graphene monolayer on WSe₂, as shown in Figure 3a. The lattice constant of the graphene/WSe₂ heterostructure is about 9.91 Å. The optimized equilibrium distance between graphene and WSe₂ is about 0.3 nm, close to the value of experiment. Figure 3b illustrates the electronic band structure and density of states (DOS) of the heterostructure. As one can see, both the gapless feature of graphene and semiconducting

nature of WSe₂ are preserved in the heterostructure. The band hybridization between the graphene and WSe₂ in the valence and conduction band regions. The gapless graphene can provides a fast channel for relaxation of photo-excited electrons in WSe₂, as illuminated by the energy diagram of the graphene/WSe₂ heterostructure (Figure 3c).

It is noteworthy that the graphene in our samples exhibits p-doping features due to the doping effect of the substrates, defects, water molecules, and oxygen in air. Meanwhile, WSe₂ has an intermediate states due to the Se-vacancies and a higher work function than graphene³⁰⁻³². Under light illumination, electrons are excited into the intermediate states (1), with photo-generated holes left in the valence bands, creating excitons in WSe₂ monolayer. Through the interlayer coupling, the photo-generated electrons transfer from the intermediate states of WSe₂ to the conduction bands of graphene (2). The photo-excited excitons relax in both graphene and WSe₂ (3). Electrons transfer from the valence band of graphene to WSe₂ monolayer to keep the neutrality of WSe₂ (4). Consequently, the graphene layer provides an additional fast channel for the recombination of photo-generated carriers in the WSe₂. Based on this unique energy band structure of graphene/WSe₂ heterostructure, it is expected that the relaxation becomes faster in graphene/WSe₂ heterostructure, which is in good agreement with experimental results in Figure 2b.

Faster relaxation in the heterostructure indicates potential applications in optoelectronic devices requiring ultrafast responses. Recently, the isolated WSe₂ and graphene have been reported to have the nonlinear saturable absorption³³⁻³⁵, which can be used as modulators for the ultrafast laser emission. It is conceivable that the graphene/WSe₂ heterostructure has unique features of the saturable absorption compared with isolated components in virtue of the interlayer coupling. We have measured the nonlinear absorptions of 2D materials (WSe₂, graphene and graphene/WSe₂ heterostructure) by the Z-scan technology. As shown in Figure 4, the saturable absorption has been observed in all samples. In order to quantitatively

determine the parameters of the saturable absorption, the nonlinear transmission is fitted by the equation below³¹.

$$T(I) = 1 - \Delta T \times e^{-\frac{I}{I_{\text{sat}}}} - T_N \quad (1)$$

Where T is the transmission, I is the excitation energy, T_N is the non-saturable absorbance, ΔT is the modulation depth, and I_{sat} is the saturation intensity. In details, for monolayer graphene $I_{\text{sat}} \approx 0.86$ GW/cm² and $\Delta T \approx 0.36$ % (Figure 4a), whilst, for the monolayer WSe₂, $I_{\text{sat}} \approx 14.1$ GW/cm² and $\Delta T \approx 0.83$ % (Figure 4b). The integration of distinct monolayers (graphene and WSe₂), ignoring the electronic tunneling, can be characterized by the product of their nonlinear transmission ($T_{\text{graphene}} \times T_{\text{WSe}_2}$) without considering the interlayer coupling effect. As shown in Figure 4c, the saturation intensity (modulation depth) of this discrete integration is 9 GW/cm² (1.2 %). This processing of the nonlinear transmission is utilized as a reference to analyze the effect of electronic tunneling to the saturation intensity of the heterostructure.

The measured nonlinear transmission of the un-irradiated graphene/WSe₂ heterostructure is also shown in Figure 4c. In comparison to that from the integration of two monolayers (graphene and WSe₂), the measured optical transmission is faster to achieve the saturation indicating the weak interlayer coupling between layers. Considering the average interlayer distance of the heterostructure ~ 4 nm in Figure 1a, weak tunneling is attributed to the long interlayer distance. Figure 4d shows the nonlinear transmission of the irradiated heterostructure (6 MeV C⁺ irradiation at the fluence of 1×10^{13} ions/cm²). After ion irradiation, the modulation depth and the saturation intensity are measured to be 2 % and 2.6 GW/cm², respectively. Compared with the integration of monolayers in Figure 4c, there is a great increasing/decreasing of the modulation depth/saturation intensity, suggesting strong interlayer coupling in the irradiated heterostructure. Figure 4e and f summarize the variation of the saturable absorption of the heterostructure as a function of the average interlayer distance. With the average thickness approaching 0.2 nm, the modulation depth and the

saturation intensity have drastic variations. Compared with the monolayer WSe₂, the saturation intensity/modulation depth of the heterostructure is decreased/increased for 3.5/1.6 times.

Since the saturable absorption of the WSe₂ is enhanced by the integration with graphene monolayer, it is interesting to apply this new heterostructure for the generation of laser pulses. We therefore apply the irradiated graphene/WSe₂ heterostructures as the saturable absorber in yttrium aluminum garnet ceramic (Nd:YAG ceramic) waveguide³⁶, which is pumped by an 810-nm laser from a continuous-wave tunable Ti:Sapphire laser. As the pump power is above 100 mW, stable laser pulses are generated by passive Q-switching. Figure 5b shows the pulse train of the output laser at the pump power of 600 mW. The pulse duration has a slow decreasing with the pumping power less than 400 mW. Above the pump power of 400 mW, the pulse duration is almost constant at 43.4 ns (Figure 5c). Figure 5d depicts the peak power of the output laser as a function of the pump power. As one can see, the peak power has a maximum value of 0.69 W. Short pulse and higher peak power are the purpose of the development of the saturable absorber. In order to explore the advantages of the heterostructure for the Q-switching, we perform a similar experiment with the monolayer WSe₂ for comparison.

With a monolayer WSe₂ (instead of the heterostructure) as a saturable absorber, the pulse train is obtained under the same pumping condition (see the data of output power, the repetition rate and the pulse duration in Figure 5e-g). As one can see, for the WSe₂ based system, the maximum peak power is 0.38W, and the minimum pulse duration is 117 ns. The peak power/pulse duration is much higher/shorter than the one obtained from the heterostructure-based system. This clearly indicates the advantage of ion irradiated graphene/WSe₂ heterostructure over WSe₂ monolayer in photonic applications.

In addition to the WSe₂ monolayer, we have also designed novel structures to optimize optical properties of WSe₂ with multilayers. As shown in Figure 6a, graphene and WSe₂

monolayer overlap with each other, constituting multilayer heterostructures (G/W×2, G/W×3). In this structure, each graphene provides an additional channel for the neighboring WSe₂ layers to accelerate the optical response. Nonlinear absorptions of G/W×2, G/W×3 are displayed in Figure 6b and c. G/W×2 has the modulation depth and the saturation intensity of 2.8% and 2.2 GW/cm², and G/W×3 has values of 3.7 % and 4 GW/cm², respectively. Compared with the G/W×1 in Figure 4, both of the saturable absorption and the modulation depth have a nearly linear increasing in the multilayer heterostructure (Figure 6c), demonstrating the stack effect of graphene/WSe₂ heterostructure.

Carbon ion irradiation has significantly enhanced the interlayer coupling of new-developed large-area graphene/WSe₂ heterostructure (consisting of monolayer graphene and WSe₂), resulting in drastic variations of nonlinear optical properties of the heterostructures. When graphene/WSe₂ spacing is modified, heterostructure possesses larger modulation depth and lower saturation intensity than each separate 2D material due to the enhanced interlayer coupling. Consequently, new Q-switched lasers have been realized by using the modified graphene/WSe₂ heterostructure as saturable absorber, showing enhanced lasing performances in respect to the monolayer WSe₂-based system. This work provides a new strategy to evaluate the quality and tailor the optical parameters of 2D heterostructures (such as black phosphorus) for particular requirements of novel photonic and optoelectronics devices.

METHODS.

Sample preparation. The graphene/WSe₂ heterostructure used in this work is produced by the chemical vapor deposition (CVD) followed by wet-chemical transfer techniques. At first, the monolayer graphene and the monolayer WSe₂ are fabricated by CVD on copper and aluminum oxide substrates, respectively. Each monolayer has a dimension of 10 mm × 10 mm. As the WSe₂ monolayer with its pristine structure has low absorption in the near-infrared (NIR) region, we

artificially tailor the atomic ratio of W and Se to 1.9 during the fabrication process, so that the intermediate states in the band gap of the WSe_2 can be generated to induce the NIR absorption. Afterwards, graphene is transferred onto the monolayer WSe_2 by the wet-chemistry transferchemical process. Due to vdW interactions, graphene and WSe_2 are bonded together to construct a graphene/ WSe_2 heterostructure. Three CVD-prepared samples of graphene/ WSe_2 heterostructures are irradiated by 6 MeV carbon (C^{3+}) ions at a fluence of 1×10^{12} ions/cm², 5×10^{12} ions/cm², and 1×10^{13} ions/cm², respectively through a 2×1.7 MV tandem accelerator at Peking University.

PL measurement. The steady-state PL and the time-resolved PL decay kinetics characterization are carried out via a PG2000-Pro-EX spectrometer. The excitation wavelength is 400 nm from the second harmonic output of a Ti:sapphire laser (Maitai HP, Spectra-Physics) at 80 MHz. The time-resolved PL measurement is performed by the time-correlated single photon-counting (TCSPC) technique and the data are collected by a Halcyone spectrometer (Ultrafast System).

Pump-probe measurement. During the measurement, the laser pulse is divided into a probe beam and a pumping beam via a beam splitter. The peak power of the probe beam is modulated as approximately 8% of the pump beam through a system of half plate and polarizer, in order to remove the nonlinear effect caused by the probe beam. The polarization of pump and probe beam is set at the magic angle to avoid anisotropic effect. The waist of the probe beam is 22 mm, which was smaller than the pump waist (152 mm). Meanwhile, we put a variable delay into the pump path and recorded the variation of the probe beam intensity versus the delay time by an energy detector after the pump beam.

DFT calculations. Our first-principles calculations were performed within density-functional theory (DFT) using the Vienna ab initio simulation package known as the VASP code^[27-29]. The electronic-ion interaction was described by projector augmented wave method (PAW)^[37,38]. The energy cutoff of the plane waves was set to 450 eV with an energy precision of 10^{-5} eV. The electron exchange–correlation function was treated using a generalized

gradient approximation (GGA) in the form proposed by Perdew, Burke, and Ernzerhof (PBE)^[39]. The vdW interactions is described by DFT-D2 method of Grimme^[40]. The Monkhorst-Pack k -point meshes^[41] for the Brillouin zone (BZ) sampling used in structural optimization and electronic structure calculations are $3 \times 3 \times 1$ and $5 \times 5 \times 1$, respectively. A vacuum region up to 15 Å was applied along the z -direction to exclude the interaction between adjacent images. Both atomic positions were fully optimized using the conjugate gradient (CG) algorithm until the maximum atomic forces were less than 0.1 eV/Å. The full relaxed lattice constant for hexagonal WSe₂ and graphene is 3.316 Å and 2.469 Å, which is consistent with previous value 3.32 Å and 2.44 Å, respectively.^[42,43] The graphene/WSe₂ heterostructure is modeled by placing a 4×4 graphene on a 3×3 WSe₂ monolayer. The slight lattice mismatch $\sim 0.67\%$ between these two lattices is neglected.

ASSOCIATED CONTENT

AUTHOR INFORMATION

Corresponding Author

**To whom correspondence should be addressed. E-mail: drfchen@sdu.edu.cn; zmw@sdu.edu.cn; hzhang@szu.edu.cn.*

Author Contributions

The manuscript was written through contributions of all authors. All authors have given approval to the final version of the manuscript.

Notes

The authors declare no competing financial interest.

ACKNOWLEDGMENT

This work is supported by the National Natural Science Foundation of China (Nos. 11535008, 21433006, and 61435010). Y. T. acknowledges the financial support from Young Scholars

Program of Shandong University (No. 2015WLJH20). Y. T. thanks suggestions from Prof.

Yinglin Song.

REFERENCES

- [1] Geim, A. K.; Grigorieva, I. V. Van der Waals heterostructures. *Nature* **2013**, 499, 419.
- [2] Ponomarenko, L. A.; Zhukov, A. K.; Geim, A. A.; Jalil, R.; Morozov, S. V.; Novoselov, K. S.; Grigorieva, I. V.; Hill, E. H.; Cheianov, V. V.; Fal'ko, V. I.; Watanabe, K.; Taniguchi, T.; Gorbachev, R. V. Tunable metal-insulator transition in double-layer graphene heterostructures. *Nat. Phys.* **2011**, 7, 958.
- [3] Haigh, S. J.; Gholinia, A.; Jalil, R.; Romani, S.; Britnell, L.; Elias, D. C.; Novoselov, K. S.; Ponomarenko, L. A.; Geim, A. K.; Gorbachev, R. Cross-sectional imaging of individual layers and buried interfaces of graphene-based heterostructures and superlattices. *Nat. Mater.* **2012**, 11, 764.
- [4] Georgiou, T.; Jalil, R.; Belle, B. D.; Britnell, L.; Gorbachev, R. V.; Morozov, S. V.; Kim, Y.; Gholinia, A.; Haigh, S. J.; Makarovskiy, O.; Eaves, L.; Ponomarenko, L. A.; Geim, A. K.; Novoselov, K. S.; Mishchenko, A. Vertical field-effect transistor based on graphene-WS₂ heterostructures for flexible and transparent electronics. *Nat. Nanotechnol.* **2012**, 8, 100.
- [5] Jariwala, D.; Marks, T. J.; Hersam, M. C. Mixed-dimensional van der Waals heterostructures. *Nat. Mater.* **2017**, 16, 170–181.
- [6] Mu, H.; Wang, Z.; Yuan, J.; Xiao, S.; Chen, C.; Chen, Y.; Chen, Y.; Song, J.; Wang, Y.; Xue, Y.; Zhang, H.; Bao, Q. Graphene–Bi₂Te₃ heterostructure as saturable absorber for short pulse generation. *ACS Photon.* **2015**, 2, 832.
- [7] Lee, C.; Lee, G.; Van der Zande, A. M.; Chen, W.; Li, Y.; Han, M.; Cui, X.; Arefe, G.; Nuckolls, C.; Heinz, T. F.; Guo, J.; Hone, J.; Kim, P. Atomically thin p–n junctions with van der Waals heterointerfaces. *Nat. Nanotechnol.* **2014**, 9, 676.
- [8] Eftekhari, E.; Li, X.; Kim, T. H.; Gan, Z.; Cole, I. S.; Zhao, D.; Kielpinski, D.; Gu, M.; Lia, Q. Anomalous Fluorescence Enhancement from Double Heterostructure 3D

- Colloidal Photonic Crystals—A Multifunctional Fluorescence-Based Sensor Platform. *Sci. Rep.* **2015**, *5*, 14439.
- [9] Britnell, L.; Gorbachev, R. V.; Jalil, R.; D Belle, B.; Schedin, F.; Mishchenko, A.; Georgiou, T.; Katsnelson, M. I.; Eaves, L.; Morozov, S. V.; Peres, N. M. R.; Leist, J.; Geim, A. K.; Novoselov, K. S.; Ponomarenko, L. A. Field-effect tunneling transistor based on vertical graphene heterostructures. *Science* **2012**, *335*, 947.
- [10] Fallahazad, B.; Lee, K.; Kang, S.; Xue, J.; Larentis, S.; Corbet, C.; Kim, K.; Movva, H. C. P.; Taniguchi, T.; Watanabe, K.; Register, L. F.; Banerjee, S. K.; Tutuc, E. Gate-tunable resonant tunneling in double bilayer graphene heterostructures. *Nano Lett.* **2015**, *15*(1), 428.
- [11] Roy, T.; Tosun, M.; Hettick, M.; Ho Ahn, G.; Hu, C.; Javey, A. Unipolar and bipolar operation of InAs/InSb nanowire heterostructure field-effect transistors. *J. Appl. Phys.* **2011**, *110*, 064510.
- [12] Obraztsov, A.; Obraztsova, E.; Tyurnina, A.; Zolotukhin, A. Chemical vapor deposition of thin graphite films of nanometer thickness. *Carbon* **2007**, *45*, 2017.
- [13] Tongay, S.; Fan, W.; Kang, J.; Park, J.; Koldemir, U.; Suh, J.; Narang, D. S.; Liu, K.; Ji, J.; Li, J.; Sinclair, R.; Wu, J. Tuning interlayer coupling in large-area heterostructures with CVD-grown MoS₂ and WS₂ monolayers. *Nano Lett.* **2014**, *14*, 3185.
- [14] Kumar, S.; Anija, M.; Kamaraju, N.; Vasu, K. S.; Subrahmanyam, K. S.; Sood, A. K.; Rao, C. N. R. Femtosecond carrier dynamics and saturable absorption in graphene suspensions. *Appl. Phys. Lett.* **2009**, *95*, 191911.
- [15] Chen, B.; Zhang, X.; Wu, K.; Wang, H.; Wang, J.; Chen, J. Q-switched fiber laser based on transition metal dichalcogenides MoS₂, MoSe₂, WS₂, and WSe₂. *Opt. Express* **2015**, *23*, 26723.
- [16] Liu, N.; Pan, Z.; Fu, L.; Zhang, C.; Dai, B.; Liu, Z. The origin of wrinkles on transferred graphene. *Nano. Res.* **2011**, *4*, 996.

- [17] Qiao, H.; Yuan, J.; Xu, Z.; Chen, C.; Lin, S.; Wang, Y.; Song, J.; Liu, Y.; Khan, Q.; Hoh, H. Y.; Pan, C.; Li, S.; Bao, Q. Broadband photodetectors based on graphene–Bi₂Te₃ heterostructure. *ACS Nano* **2015**, *9*, 1886.
- [18] Wang, Y.; Zhang, Y.; Lu, Y.; Xu, W.; Mu, H.; Chen, C.; Qiao, H.; Song, J.; Li, S.; Sun, B.; Cheng, Y.; Bao, Q. Hybrid graphene–perovskite phototransistors with ultrahigh responsivity and gain. *Adv. Opt. Mater.* **2015**, *3*, 1389.
- [19] B. Guo, Q. Liu, E. Chen, H. Zhu, L. Fang, J. R. Gong, Can graphene be used as a substrate for Raman enhancement?. *Nano.Lett.* **2010**, *10*, 553–561.
- [20] Kim, J.; Hwang, J. H.; Suh, J.; Tongay, S.; Kwon, S.; Hwang, C. C.; Wu, J.; Park, J. Y. Work function engineering of single layer graphene by irradiation-induced defects. *Appl. Phys. Lett.* **2013**, *103*, 171604.
- [21] Hashimoto, A.; Suenaga, K.; Gloter, A.; Urita, K.; Iijima, S. Direct evidence for atomic defects in graphene layers. *Nature* **2004**, *430*, 870.
- [22] Sahin, H.; Tongay, S.; Horzum, S.; Fan, W.; Zhou, J.; Li, J.; Wu, J.; Peeters, F. M. Anomalous Raman spectra and thickness-dependent electronic properties of WSe₂. *Phys. Rev. B* **2013**, *87*(16), 165409.
- [23] Huang, Y.; Wu, J.; Hwang, K. C. Thickness of graphene and single-wall carbon nanotubes. *Phys. Rev. B* **2006**, *74*, 245413.
- [24] S. M. Clark, K. Jeon, J. Y. Chen and C. S. Yoo., Few-layer graphene under high pressure: Raman and X-ray diffraction studies. *Solid State Commun.* **2013**, *154*, 15–18.
- [25] Zhao, W.; Ghorannevis, Z.; Chu, L.; Toh, M.; Kloc, C.; Tan, P.; Eda, G. Evolution of electronic structure in atomically thin sheets of WS₂ and WSe₂. *ACS Nano* **2013**, *7*, 791.
- [26] Xia, T.; Dogariu, A.; Mansour, K.; Hagan, D. J.; Said, A. A.; Van Stryland, E. W. and Shi S., Nonlinear response and optical limiting in inorganic metal cluster Mo₂Ag₄S₈ (PPh₃)₄ solutions. *J. Opt. Soc. Am. B* **1998**, *15*, 1497.

- [27]Kress, G. and Furthmuller, J. Efficiency of ab-initio total energy calculations for metals and semiconductors using a plane-wave basis set. *Comput. Mater. Sci.* **1996**, 6, 15.
- [28]Kresse, G. and Hafner, J. Ab initio molecular dynamics for liquid metals. *Phys. Rev. B* **1993**, 47, 558.
- [29]Kresse, G. and Hafner, J. Ab initio molecular dynamics for open-shell transition metals. *Phys. Rev. B* **1993**, 48, 13115.
- [30]Du, J.; Wang, Q.; Jiang, G.; Xu, C.; Zhao, C.; Xiang, Y.; Chen, Y.; Wen, S.; Zhang, H. Ytterbium-doped fiber laser passively mode locked by few-layer Molybdenum Disulfide (MoS₂) saturable absorber functioned with evanescent field interaction. *Sci. Rep.* **2014**, 4, 6346.
- [31]Liu, C.; Chang, Y.; Norris, T. B.; Zhong, Z. Graphene photodetectors with ultra-broadband and high responsivity at room temperature. *Nat. Nanotechnol.* **2014**, 9, 273.
- [32]Di Bartolomeo, A. Graphene Schottky diodes: An experimental review of the rectifying graphene/semiconductor heterojunction. *Phys. Rep.* **2016**, 8, 1-58.
- [33]Chen, B.; Zhang, X.; Wu, K.; Wang, H.; Wang, J.; Chen, J. Q-switched fiber laser based on transition metal dichalcogenides MoS₂, MoSe₂, WS₂, and WSe₂. *Opt. Express* **2015**, 23, 26723.
- [34]Zhang, H.; Tang, D.; Knize, R. J.; Zhao, L.; Bao, Q.; Loh, K. P. Graphene mode locked, wavelength-tunable, dissipative soliton fiber laser. *Appl. Phys. Lett.* **2010**, 96, 111112.
- [35]Bao, Q.; Zhang, H.; Wang, Y.; Ni, Z.; Yan, Y.; Shen, Z. X.; Loh, K. P.; Tang, D. Y. Atomic - layer graphene as a saturable absorber for ultrafast pulsed lasers. *Adv. Fun. Mater.* **2009**, 19, 3077.
- [36]Tan, Y.; Akhmadaliev, S.; Zhou, S.; Sun, S.; Chen, F. Guided continuous-wave and graphene-based Q-switched lasers in carbon ion irradiated Nd: YAG ceramic channel waveguide. *Opt. Express* **2014**, 22, 3572.

- [37]Kresse, G. and Joubert, D. From ultrasoft pseudopotentials to the projector augmented-wave method. *Phy. Rev. B* **1999**, 59, 1758.
- [38] Kresse, G. and Furthmuller, J. Efficient iterative schemes for ab initio total-energy calculations using a plane-wave basis set. *Phy. Rev. B* **1996**, 54, 11169.
- [39]Perdew, J. P.; Burke, K.; Ernzerhof, M. Generalized gradient approximation made simple. *Phys. Rev. Lett.* **1996** 77, 3865.
- [40]Grimme,S.; Semiempirical GGA - type density functional constructed with a long - range dispersion correction. *Comput. J. Chem.* **2006** 27, 1787.
- [41]Monkhorst, H. J. and Pack, J. D. Special points for Brillouin-zone integrations. *Phys. Rev. B* **1976** 13, 5188.
- [42]Ramasubramaniam, A. Large excitonic effects in monolayers of molybdenum and tungsten dichalcogenides. *Phy. Rev. B* **2012** 86.
- [43]Xu, Z. and Buehler, M. J. Interface structure and mechanics between graphene and metal substrates: a first-principles study. *J. Phys. Conden. Matt.* **2010**, 22, 485301.

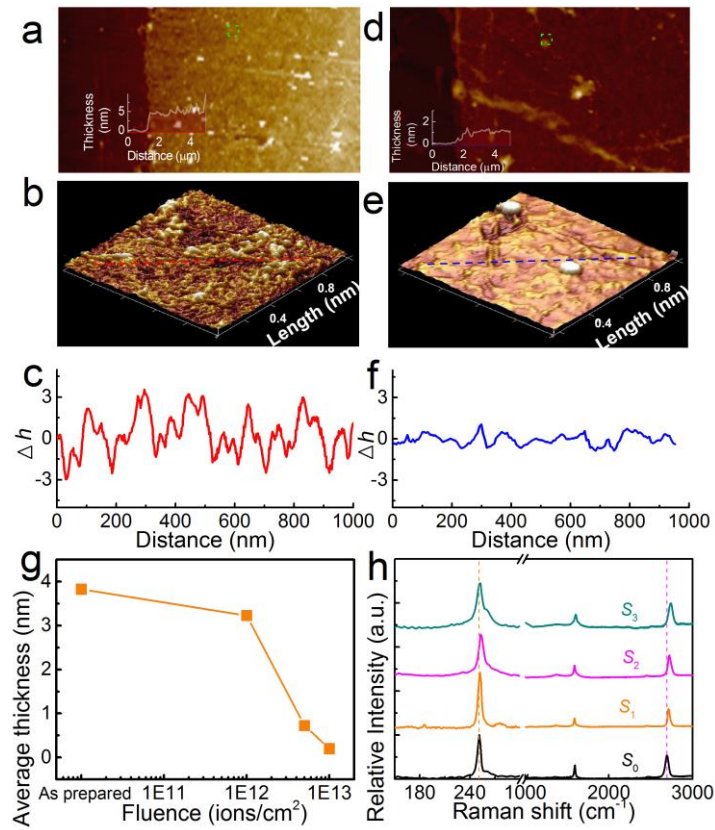


Figure 1. Morphology of the graphene/WSe₂ heterostructure before a) and after d) the ion irradiation captured by the AFM. b) and e) are the enlarged views of green squares in a) and d). c) and f) are the thickness variation along the red and blue lines in b) and e). g) The variation of the thickness of the graphene/WSe₂ heterostructures as a function of the fluence of the carbon ion beam. h) is Raman spectrum of the graphene/WSe₂ heterostructure before and after the ion irradiation.

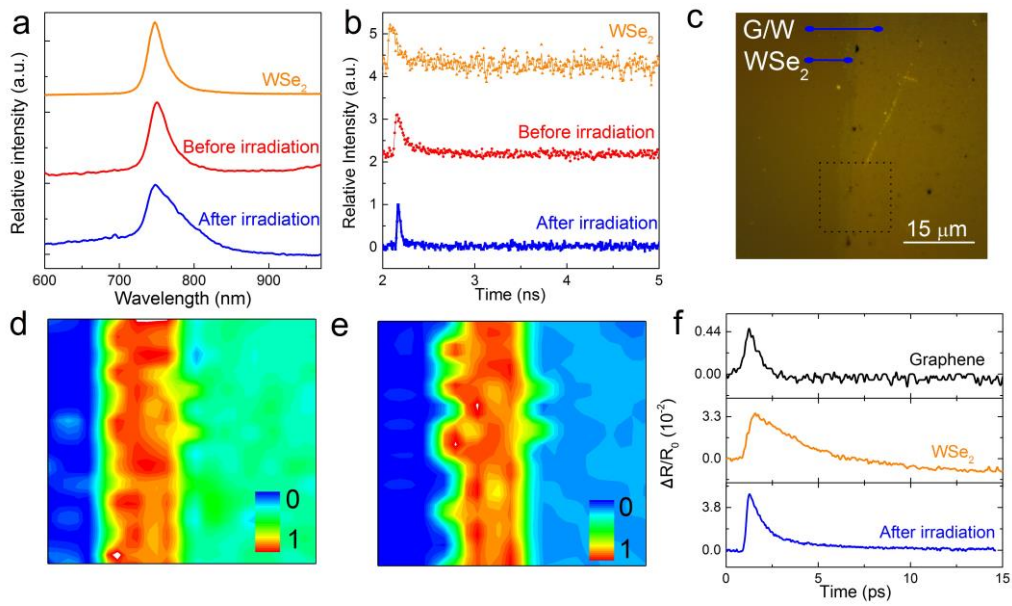


Figure 2. a) PL spectra, b) PL decay curves, c) Microscope photo of the G/W heterostructure. PL mappings of G/W heterostructure in the black square of c) before d) and after e) ion irradiation. f) single-exponential decay curves of WSe₂, graphene/WSe₂ heterostructure before and after the ion irradiation.

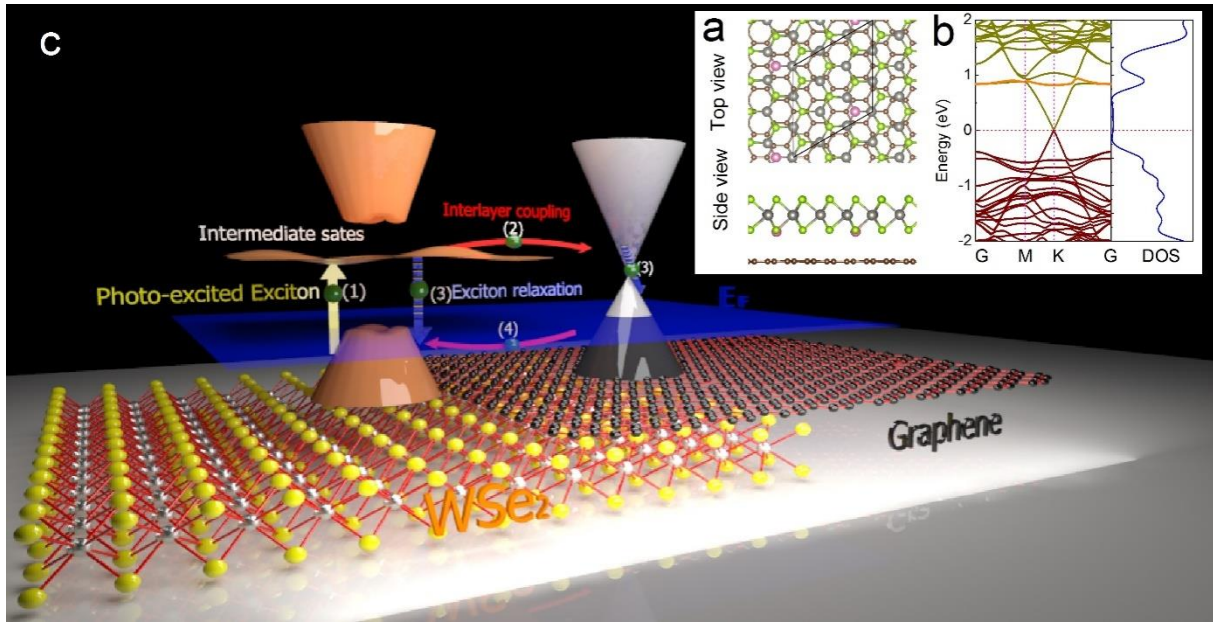


Figure 3. a) Geometry (top and side view) and b) electronic band structure and DOS of the graphene/WSe₂ heterostructure. The flat band marked in orange indicates the intermediate states induced by Se-vacancies. c) Schematic diagram showing electronic transitions in graphene/WSe₂ heterostructure.

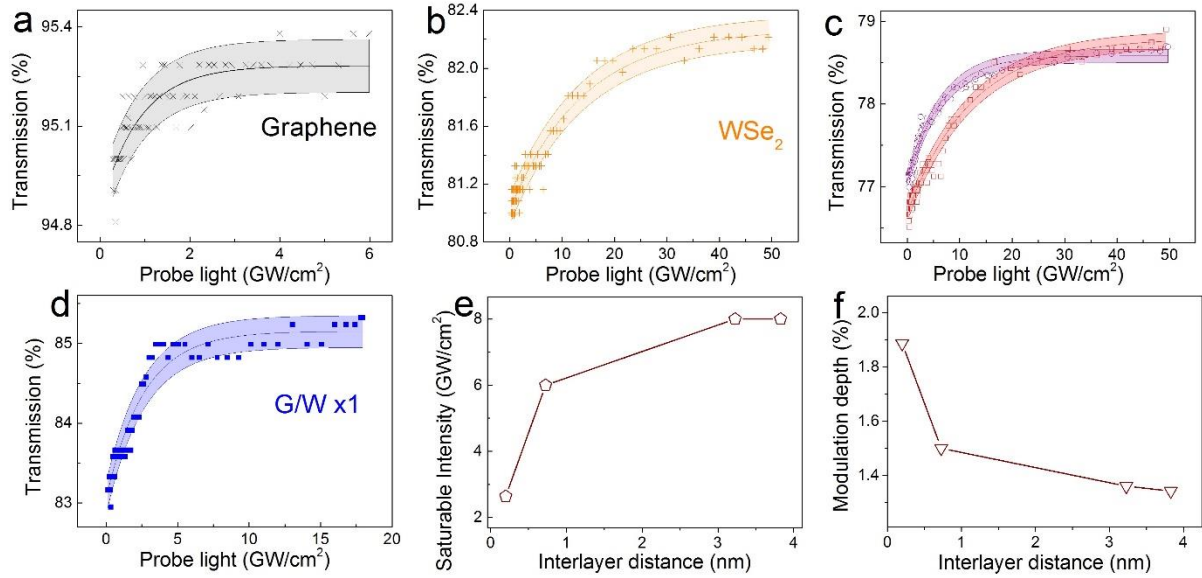


Figure 4. Nonlinear transmission of a) monolayer graphene, b) monolayer WSe₂, c) as-prepared graphene/WSe₂ heterostructure, and d) irradiated graphene/WSe₂ heterostructure measured by the Z-scan technology at the wavelength of 1064 nm. The nonlinear transmission product of monolayer graphene and monolayer WSe₂ are shown in c) as Cyan squares. Variation of the modulation depth e) and the saturation intensity f) of the graphene/WSe₂ heterostructure along with the thickness of the graphene/WSe₂ heterostructure.

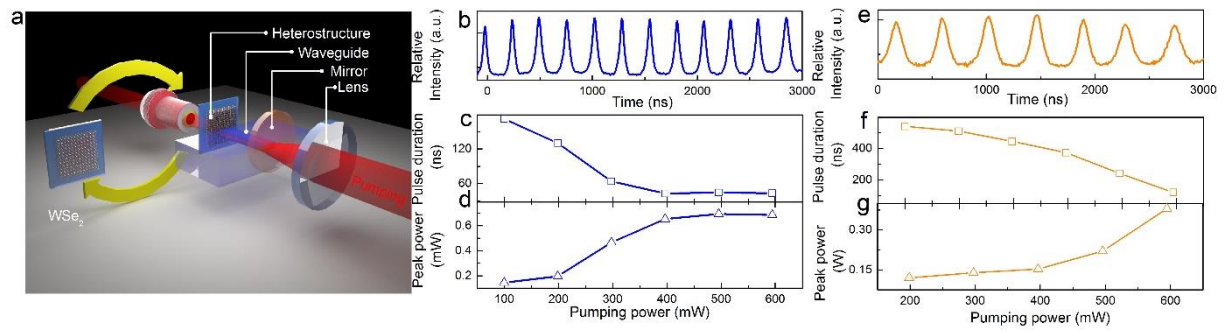


Figure 5. a) Experimental setup for the Q-switched waveguide laser. The b) pulse train, c) output power, and d) repetition rate and pulse duration of the output laser modulated by the graphene/WSe₂ heterostructure. The e) pulse train, f) output power, g) repetition rate and pulse duration of the output laser modulated by the monolayer WSe₂.